

---

# Quantum Kernel Mixtures for Probabilistic Deep Learning

---

**Fabio A. González**  
MindLab  
Universidad Nacional de Colombia  
Bogotá, Colombia  
fagonzalezo@unal.edu.co

**Raúl Ramos-Pollán**  
Universidad de Antioquia  
Medellín, Colombia  
raul.ramos@udea.edu.co

**Joseph A. Gallego-Mejía**  
MindLab  
Universidad Nacional de Colombia  
Bogotá, Colombia  
jagallegom@unal.edu.co

## Abstract

This paper presents a novel approach to probabilistic deep learning (PDL), quantum kernel mixtures, derived from the mathematical formalism of quantum density matrices, which provides a simpler yet effective mechanism for representing joint probability distributions of both continuous and discrete random variables. The framework allows for the construction of differentiable models for density estimation, inference, and sampling, enabling integration into end-to-end deep neural models. In doing so, we provide a versatile representation of marginal and joint probability distributions that allows us to develop a differentiable, compositional, and reversible inference procedure that covers a wide range of machine learning tasks, including density estimation, discriminative learning, and generative modeling. We illustrate the broad applicability of the framework with two examples: an image classification model, which can be naturally transformed into a conditional generative model thanks to the reversibility of our inference procedure; and a model for learning with label proportions, which is a weakly supervised classification task, demonstrating the framework's ability to deal with uncertainty in the training samples.

## 1 Introduction

Probabilistic deep learning (PDL) refers to the combination of deep neural networks and probabilistic models. PDL can model uncertainty on the input data, the output predictions and/or the model parameters. Examples of PDL methods include deep Gaussian processes (DGP) [1], Bayesian neural networks (BNN) [2], generative adversarial networks (GANs) [3], variational autoencoders [4], and autoregressive models. The different methods present different approaches to PDL. DGP models the entire training dataset as a stochastic process, while BNN uses a Bayesian approach to model the neural network parameters. Some methods focus on a particular task, such as GANs, which are designed for generation, while others are more versatile and can support a wide range of tasks. Normalizing flows (NF) [5, 6] are an example of the latter and can be applied to tasks such as density estimation, sampling, variational inference, clustering, and classification. The strength of this method lies in its ability to represent complex continuous probability distributions.

The framework presented in this paper follows a similar approach but using a novel simpler mechanism to represent both continuous and discrete probability distributions: quantum kernel mixtures. The framework can be used for building models for density estimation, inference and sampling that are differentiable, and therefore could be integrated in end-to-end deep neural models. The concept of quantum kernel mixture is derived from the quantum mechanics concept of density matrix, which describes the statistical state of a quantum system. A quantum kernel mixture can be seen as either a density matrix in a reproducing kernel Hilbert space (RKHS) or as a generalization of non-parametric density estimation methods (such as kernel density estimation) for representing probability distributions.

Density matrices are an appealing mechanism to represent probability distributions in machine learning. Few works have explored their applications to some machine learning tasks: classification [7, 8], clustering [9], and multimodal learning [10] are some examples. The two works closest to the present study are those of Srinivasan et al. [11] and González et al. [12]. Srinivasan et al. [11] show how density matrices, implicitly embedded in a Hilbert space by a kernel, can be used to model continuous probability distributions in graphical models. González et al. [12] combine density matrices with Random Fourier Features (RFF) [13] to represent probability distributions, perform inference, and integrate them into deep learning models.

The primary contributions of this paper include: (i) a versatile mechanism, quantum kernel mixture (QKM), for representing both continuous and discrete probability distributions, which can be integrated with deep architectures to tackle various learning tasks; (ii) a method for conducting inference using quantum kernel mixtures that is differentiable, compositional, and reversible; (iii) an examination of the framework’s capabilities in diverse learning tasks.

## 2 Density matrices and quantum kernel mixtures

### 2.1 Density matrices

A wave function, denoted as  $|\psi\rangle$ , is a complex-valued function that lives in a Hilbert space,  $\mathcal{H}$ , and provides a complete description of the state of a ‘pure’ quantum system. The probability of finding a system in a particular state is given by the square of the absolute value of the projection of the wave function onto the desired state (also called the probability amplitude). This is known as the Born rule [14].

In addition to the quantum uncertainty represented by the wave function, it is possible for the system to have classical uncertainty. In this case we say that the system is in a ‘mixed’ state, i.e. a statistical mixture of different states,  $|\psi_i\rangle$ , each with an associated probability  $p_i$ , with  $\sum_i^N p_i = 1$ . This is represented by a density matrix,  $\rho$ , which is the more general way to represent the state of a quantum system:

$$\rho = \sum_i^N p_i |\psi_i\rangle\langle\psi_i| \tag{1}$$

where  $\langle\psi_i|$  represents the conjugate transpose of  $|\psi_i\rangle$ . A density matrix is a Hermitian, positive-semidefinite matrix with unit trace, defined on the Hilbert space associated with the quantum system<sup>1</sup>. The Born rule can be extended to compute the probability of finding a system with the state represented by  $\rho$  in a state  $|\psi\rangle$  after a measurement:

$$p(|\psi\rangle|\rho) = \text{Tr}(|\psi\rangle\langle\psi|\rho) = \langle\psi|\rho|\psi\rangle = \sum_i^N p_i |\langle\psi|\psi_i\rangle|^2 \tag{2}$$

Density matrices are a powerful mechanism to represent quantum probability distributions and efficiently perform different calculations: outcomes of quantum measurements, expected values, properties of composite systems, and system dynamics, among others [14].

---

<sup>1</sup>The Hilbert space may be infinite dimensional, in which case we speak of density operators instead of density matrices.

The following section introduces the concept of a QKM, which can be thought of as a density matrix defined in the RKHS induced by a kernel. In this work, QKMs are used to efficiently represent joint probability distributions and to perform inference, among other things. The defined operations are differentiable and therefore integrable into deep learning models.

## 2.2 Quantum kernel mixtures

**Definition 2.1** (Quantum kernel mixture). A quantum kernel mixture over a set  $\mathbb{X}$  is a triplet  $\rho = (\mathbf{C}, \mathbf{p}, k_\theta)$  where  $\mathbf{C} = \{\mathbf{x}^{(1)}, \dots, \mathbf{x}^{(m)}\} \subseteq \mathbb{X}$ ,  $\mathbf{p} = (p_1, \dots, p_m) \in \mathbb{R}^m$  and  $k_\theta : \mathbb{X} \times \mathbb{X} \rightarrow \mathbb{R}$ , such that  $\forall \mathbf{x} \in \mathbb{X}$ ,  $k(\mathbf{x}, \mathbf{x}) = 1$ ,  $\forall i$   $p_i \geq 0$  and  $\sum_{i=1}^m p_i = 1$ .

The elements of  $\mathbf{C}$  are the components of the QKM, and the  $p_i$  value represents the mixture weight, or probability, of the component  $\mathbf{x}_i$ . If  $\phi : \mathbb{R}^n \rightarrow \mathcal{H}$  is the mapping to the RKHS  $\mathcal{H}$  associated to the kernel  $k_\theta$ ,  $\rho$  represents a density matrix defined as in (1) with components  $|\psi_i\rangle = |\phi(\mathbf{x}^{(i)})\rangle$ . The projection function associated to a QKM  $\rho$  is defined as:

$$f_\rho(\mathbf{x}) = \sum_{\mathbf{x}^{(i)} \in \mathbf{C}} p_i k_\theta^2(\mathbf{x}, \mathbf{x}^{(i)}) \quad (3)$$

If we replace  $k_\theta^2(\mathbf{x}, \mathbf{x}^{(i)})$  by  $|\langle \phi(\mathbf{x}) | \phi(\mathbf{x}^{(i)}) \rangle|^2$  in (3), we get the Born rule equation (2). In quantum mechanics it is common to work with complex Hilbert spaces, in this work we use real-valued kernels over a real domain. This implies that the represented density matrices live in a real Hilbert space. This framework can be easily extended to the complex case, but the real case is sufficient for our goal of representing classical probability distributions.

A central idea in this work is that the projection function in (3) can be transformed in a probability density function (PDF) by multiplying it by a normalization constant that depends on the kernel of the QKM:

$$\hat{f}_\rho(\mathbf{x}) = \mathcal{M}_k f_\rho(\mathbf{x}) \quad (4)$$

**Continuous distributions.** For representing continuous probability distributions, we will use the Gaussian (or RBF) kernel,  $k_{\text{rbf}, \sigma}(\mathbf{x}, \mathbf{y}) = e^{-\frac{\|\mathbf{x} - \mathbf{y}\|^2}{2\sigma^2}}$ .

A QKM  $\rho_{\mathbf{x}} = (\mathbf{C}, \mathbf{p}, k_{\text{rbf}})$  with  $\mathbf{C} \subseteq \mathbb{R}^n$  represents a continuous probability distribution<sup>2</sup> of a random variable  $\mathbf{x} \in \mathbb{R}^n$  with a PDF given by (4) with normalizing constant  $\mathcal{M}_{k_{\text{rbf}}} = \frac{1}{\sqrt{(2\pi)^n (\sqrt{2}\sigma)^n}}$ .

It is not difficult to check that the PDF corresponding to  $\rho_{\mathbf{x}}$ ,  $\hat{f}_{\rho_{\mathbf{x}}}$ , is a valid PDF over  $\mathbb{R}^n$ . In fact, (4), with normalizing constant  $\mathcal{M}_{k_{\text{rbf}}}$ , is a generalization of the non-parametric estimation approach to density estimation with kernels known as kernel density estimation (KDE) [15, 16]. As shown in the present work, QKMs can be used in wider range of applications and can be learned using non-parametric and parametric approaches.

**Discrete distributions.** For discrete probability distributions we use the cosine kernel,  $k_{\text{cos}}(\mathbf{x}, \mathbf{y}) = \frac{\langle \mathbf{x}, \mathbf{y} \rangle}{\sqrt{\langle \mathbf{x}, \mathbf{x} \rangle \langle \mathbf{y}, \mathbf{y} \rangle}}$ , with the normalization constant  $\mathcal{M}_{k_{\text{cos}}} = 1$ . The following proposition shows that a QKM  $\rho_{\mathbf{x}} = (\mathbf{C}, \mathbf{p}, k_{\text{cos}})$  represents a probability distribution for a random variable  $\mathbf{x}$  that can take a finite set of values.

**Proposition 2.2.** *Let  $\rho_{\mathbf{x}} = (\mathbf{C}, \mathbf{p}, k_{\text{cos}})$  be a QKM over  $\mathbb{R}^n$ ; let  $\mathbb{X} = \{\mathbf{b}^{(1)}, \dots, \mathbf{b}^{(n)}\} \subset \mathbb{R}^n$  be an orthogonal basis of  $\mathbb{R}^n$ , then  $\{f_\rho(\mathbf{b}^{(i)})\}_{i=1, \dots, n}$  is a categorical probability distribution for the random variable  $\mathbf{x} \in \mathbb{X}$ .*

In particular, if we use the canonical basis  $\mathbb{X} = \{\mathbf{e}^{(1)}, \dots, \mathbf{e}^{(n)}\}$ , the function in (4), defines a valid categorical PDF over  $\mathbb{X}$ :

$$\hat{f}_{\rho_{\mathbf{x}}}(\mathbf{x}) = f_{\rho_{\mathbf{x}}}(\mathbf{x}), \text{ for } \mathbf{x} \in \{\mathbf{e}^{(i)}\}_{i=1 \dots n} \quad (5)$$

As an example, consider the discrete probability distribution  $\mathbf{p} = (0.2, 0.3, 0.5)$ . It can be represented by the QKM  $\rho_0 = (\{(1, 0, 0), (0, 1, 0), (0, 0, 1)\}, (0.2, 0.3, 0.5), k_{\text{cos}})$ , also, it can be represented by the QKM  $\rho_1 = (\{(\sqrt{0.2}, \sqrt{0.3}, \sqrt{0.5})\}, (1), k_{\text{cos}})$ .

<sup>2</sup>We will use the notation  $\rho_{\mathbf{x}}$  to indicate that the QKM  $\rho$  represents a probability distribution for the random variable  $\mathbf{x}$ .

Of course, it is possible to extend the results to other kernels as long as the corresponding density function is a valid PDFs based on (4).

### 2.3 Density estimation with quantum kernel mixtures

Since a QKM extends the notion of kernel density estimator, it is possible to perform non-parametric density estimation with QKMs. In fact, Equation 4 corresponds to a KDE density estimator with a Gaussian kernel and a bandwidth parameter  $\sqrt{2}\sigma$ . The following theorem guarantees that the estimator in (4) converges in probability to the real PDF:

**Theorem 2.3** (Parzen [16]). *Let  $\mathbf{D} = \{\mathbf{x}^{(1)}, \dots, \mathbf{x}^{(\ell)}\} \subseteq \mathbb{R}^n$  be a set of iid samples drawn from a probability distribution with PDF  $f$ ; let  $\rho_{\mathbf{x}}^{\ell} = (\mathbf{D}, \mathbf{p} = \{\frac{1}{\ell}, \dots, \frac{1}{\ell}\}, k_{\text{rbf}, \sigma_{\ell}})$  be a QKM; and let  $\hat{f}_{\rho_{\mathbf{x}}^{\ell}}$  be defined as in (4). Assume that  $f$  is continuous at  $\mathbf{x}$  and that  $\sigma_{\ell} \rightarrow 0$  and  $\ell\sigma_{\ell} \rightarrow \infty$  as  $\ell \rightarrow \infty$ . Then  $\hat{f}_{\rho_{\mathbf{x}}^{\ell}}(\mathbf{x}) \xrightarrow{P} f(\mathbf{x})$ .*

The following proposition corresponds to the analogous result for categorical probability distributions.

**Proposition 2.4.** *Let  $\mathbb{X} = \{\mathbf{e}^{(1)}, \dots, \mathbf{e}^{(n)}\}$  be the canonical basis of  $\mathbb{R}^n$ ; let  $\mathbf{D} = \{x_1, \dots, x_{\ell}\} \subseteq \mathbb{R}^n$  be a set of iid samples drawn from  $\mathbb{X}$  with categorical probability distribution  $\mathbf{p} = (p_1, \dots, p_n)$ ; let  $\rho_{\mathbf{x}}^{\ell} = (\mathbf{D}, \mathbf{p} = (\frac{1}{\ell}, \dots, \frac{1}{\ell}), k_{\text{cos}})$  be a QKM; and let  $\hat{f}_{\rho_{\mathbf{x}}^{\ell}}(i)$  be defined as in (5). Then  $\hat{f}_{\rho_{\mathbf{x}}^{\ell}}(i) \rightarrow p_i$  as  $\ell \rightarrow \infty$ .*

It is also possible to perform parametric density estimation by maximizing the likelihood of the QKM parameters given a training dataset. Given a QKM with  $K$  components  $\rho = (\mathbf{C} = \{\mathbf{c}^{(1)}, \dots, \mathbf{c}^{(K)}\}, \mathbf{p} = \{p_1, \dots, p_K\}, k_{\theta})$ , where  $\theta$  indicate a set of parameters of the kernel, and a training data set  $\mathbf{D} = \{\mathbf{x}_1, \dots, \mathbf{x}_{\ell}\}$ , solving the following optimization problem:

$$\max_{\mathbf{C}, \mathbf{p}, \theta} \sum_{i=1}^{\ell} \log \hat{f}_{\rho}(x_i) \quad (6)$$

will find a QKM that maximizes the probability density of the samples in  $\mathbf{D}$ . For the cosine or RBF kernels, or for joint mixtures of these kernels, this is equivalent to perform maximum likelihood estimation.<sup>3</sup>

### 2.4 Joint densities with quantum kernel mixtures

In quantum mechanics, the state of a bipartite system with subsystems  $A$  and  $B$  is represented by a density matrix in the tensor product Hilbert space  $\mathcal{H}_A \otimes \mathcal{H}_B$ , where  $\mathcal{H}_A$  and  $\mathcal{H}_B$  are the representation spaces of  $A$  and  $B$  respectively [14]. Following the same line of thought, a joint QKM for random variables  $\mathbf{x} \in \mathbb{X}$  and  $\mathbf{y} \in \mathbb{Y}$  is defined as follows:  $\rho_{\mathbf{x}, \mathbf{y}} = (\mathbf{C}, \mathbf{p}, k_{\mathbb{X}} \otimes k_{\mathbb{Y}})$  where  $\mathbf{C} \subseteq \mathbb{X} \times \mathbb{Y}$ ,  $k_{\mathbb{X}}$  and  $k_{\mathbb{Y}}$  are kernels over  $\mathbb{X}$  and  $\mathbb{Y}$  respectively, and  $k_{\mathbb{X}} \otimes k_{\mathbb{Y}}((\mathbf{x}, \mathbf{y}), (\mathbf{x}', \mathbf{y}')) = k_{\mathbb{X}}(\mathbf{x}, \mathbf{x}')k_{\mathbb{Y}}(\mathbf{y}, \mathbf{y}')$ . If  $\mathcal{M}_{k_{\mathbb{X}}}$  and  $\mathcal{M}_{k_{\mathbb{Y}}}$  are the normalizing constants corresponding to the kernels  $k_{\mathbb{X}}$  and  $k_{\mathbb{Y}}$  respectively, the normalizing constant for  $k_{\mathbb{X}} \otimes k_{\mathbb{Y}}$  in (4) is  $\mathcal{M}_{k_{\mathbb{X}} \otimes k_{\mathbb{Y}}} = \mathcal{M}_{k_{\mathbb{X}}}\mathcal{M}_{k_{\mathbb{Y}}}$ . It is also possible to easily calculate a marginal QKM from a joint QKM. Suppose that  $k_{\mathbb{X}} = k_{\text{rbf}}$ , then a marginal QKM  $\rho_{\mathbf{y}}$  must satisfy:

$$\hat{f}_{\rho_{\mathbf{y}}}(\mathbf{y}) = \int \hat{f}_{\rho_{\mathbf{x}, \mathbf{y}}}(\mathbf{x}, \mathbf{y})d\mathbf{x} = \int \sum_i p_i \mathcal{M}_{k_{\mathbb{X}}} \mathcal{M}_{k_{\mathbb{Y}}} k_{\mathbb{X}}^2(\mathbf{x}^{(i)}, \mathbf{x}) k_{\mathbb{Y}}^2(\mathbf{y}^{(i)}, \mathbf{y})d\mathbf{x} = \sum_i p_i \mathcal{M}_{k_{\mathbb{Y}}} k_{\mathbb{Y}}^2(\mathbf{y}^{(i)}, \mathbf{y}) \quad (7)$$

It is not difficult to see that  $\rho_{\mathbf{y}} = (\{\mathbf{y}^{(i)} | (\mathbf{x}^{(i)}, \mathbf{y}^{(i)}) \in \mathbf{C}\}, \mathbf{p}, k_{\mathbb{Y}})$  satisfies 7. The same argument applies for defining  $\rho_{\mathbf{x}}$ . For  $k_{\mathbb{X}} = k_{\text{cos}}$ , we replace the integral in (7) by a sum over a basis (see Proposition 2.2) to obtain an analogous result.

### 2.5 Inference with quantum kernel mixtures

Inference aims to estimate unknown output variables from known input variables and a model's parameters. A probabilistic approach models the input-output relationship as a probability distribution,

<sup>3</sup>The optimization problem in (6) could be ill-posed, e.g. for the RBF kernel, (6) could get arbitrary large values if one sample  $\mathbf{x}_i$  coincides with one of the kernel mixture components and the  $\sigma$  parameter of the kernel goes to zero. This could be dealt with using techniques such as restricted optimization or regularization.

e.g.,  $p(\mathbf{x}', \mathbf{y}')$ , which reflects uncertainty about the training data-generation process. Additional uncertainty may arise from imprecise input data during prediction, which can be modeled as a probability distribution over the input domain,  $p(\mathbf{x})$ . Note that we use a different random variable,  $\mathbf{x}$ , to represent a new input fed to the trained model during prediction, than the random variable used to represent input training samples,  $\mathbf{x}'$ . In general,  $p(\mathbf{x}) \neq \int p(\mathbf{x}', \mathbf{y}' = \mathbf{y}) d\mathbf{y}$ . When predicting output variables, both sources of uncertainty need to be considered and reflected in the output distribution,  $p(\mathbf{y})$ . Inference transforms a probability distribution of input variables,  $p(\mathbf{x})$ , into a distribution of output variables,  $p(\mathbf{y})$ , using a joint probability of inputs and outputs,  $p(\mathbf{x}', \mathbf{y}')$ .

We will demonstrate how this process can be modeled using quantum kernel mixtures. Each one of the probability distributions  $p(\mathbf{x})$ ,  $p(\mathbf{x}', \mathbf{y}')$  and  $p(\mathbf{y})$  are represented by QKMs as follows:

$$\rho_{\mathbf{x}} = (\{\mathbf{x}^{(i)}\}_{i=1\dots m}, (p_i)_{i=1\dots m}, k_{\mathbb{X}}) \quad (8)$$

$$\rho_{\mathbf{x}', \mathbf{y}'} = (\{\mathbf{x}'^{(i)}, \mathbf{y}'^{(i)}\}_{i=1\dots m'}, (p'_i)_{i=1\dots m'}, k_{\mathbb{X}} \otimes k_{\mathbb{Y}}) \quad (9)$$

$$\rho_{\mathbf{y}} = (\{\mathbf{y}'^{(i)}\}_{i=1\dots m'}, (p''_i)_{i=1\dots m'}, k_{\mathbb{Y}}) \quad (10)$$

Notice that if we have a unique input sample  $\mathbf{x}$ ,  $\rho_{\mathbf{x}}$  would have only one component. In general, we have a probability distribution represented by the QKM  $\rho_{\mathbf{x}}$  with  $m$  components. Also, note that  $k_{\mathbb{X}}$  in  $\rho_{\mathbf{x}}$ , is the same kernel as in  $\rho_{\mathbf{x}', \mathbf{y}'}$ . Likewise,  $k_{\mathbb{Y}}$  in  $\rho_{\mathbf{y}}$ , is the same kernel as in  $\rho_{\mathbf{x}', \mathbf{y}'}$ . Also, the  $\mathbf{y}'^{(i)}$  components of the quantum kernel mixture  $\rho_{\mathbf{y}}$  are same as the ones of the QKM  $\rho_{\mathbf{x}', \mathbf{y}'}$ . The probabilities of the inferred  $\rho_{\mathbf{y}}$  quantum kernel mixture are given by the following expression:

$$p''_i = \sum_{\ell=1}^m \frac{p_{\ell} p'_i (k_x(\mathbf{x}^{(\ell)}, \mathbf{x}'^{(i)}))^2}{\sum_{j=1}^{m'} p'_j (k_x(\mathbf{x}^{(\ell)}, \mathbf{x}'^{(j)}))^2}, \text{ for } i = 1 \dots m' \quad (11)$$

The time complexity of the inference process given by (11) is  $O(mm'n)$  where  $n$  is the dimension of the input space. This inference procedure is similar to Nadaraya-Watson kernel regression (NWKR) [17, 18], which uses a kernel function to assign local weights to each output training sample according to the input sample's similarity with each input training sample. However, NWKR only produces a point estimate of the output variable, while we obtain a full probability distribution represented as a QKM.

In addition to its expressiveness and flexibility, kernel-mixture-based inference has two advantages:

- **Compositionality.** Given two joint QKMs  $\rho_{\mathbf{x}', \mathbf{y}'}$  and  $\rho_{\mathbf{y}', \mathbf{z}'}$  and input QKM  $\rho_{\mathbf{x}}$ , we can infer  $\rho_{\mathbf{y}}$  from  $(\rho_{\mathbf{x}', \mathbf{y}'}, \rho_{\mathbf{x}})$  and then infer  $\rho_{\mathbf{z}}$  from  $(\rho_{\mathbf{y}', \mathbf{z}'}, \rho_{\mathbf{y}})$ .
- **Reversibility.** Thanks to the symmetry of the joint QKMs  $\rho_{\mathbf{x}', \mathbf{y}'}$ , it can be used to infer  $\rho_{\mathbf{x}}$  from  $\rho_{\mathbf{y}}$  as well as to infer  $\rho_{\mathbf{y}}$  from  $\rho_{\mathbf{x}}$ .

From the point of view of quantum mechanics,  $\rho_{\mathbf{x}', \mathbf{y}'}$  is a density matrix representing the state of a bipartite system, and the inference process corresponds to a measurement operation that collapses the  $\mathbf{x}$  subsystem to a state  $\rho_{\mathbf{x}}$ . This collapse affects the  $\mathbf{y}$  subsystem whose state is changed to be  $\rho_{\mathbf{y}}$ . With density matrices, this process corresponds to applying a collapse operator to  $\rho_{\mathbf{x}', \mathbf{y}'}$  and computing a partial trace [12]. With our QKM representation, this process is efficiently done by (11).

The following proposition shows that the probabilities assigned by (11) generate a QKM that is equivalent to the one calculated by Bayesian inference.

**Proposition 2.5.** *Let  $\mathbf{x}'$  and  $\mathbf{y}'$  be random variables with joint a joint probability distribution represented by a QKM mixture  $\rho_{\mathbf{x}', \mathbf{y}'}$  (Eq. (9)), and let  $\rho_{\mathbf{x}}$  be the QKM defined by (8)), then the kernel mixture  $\rho_{\mathbf{y}}$  (Eq. (10) and Eq. 11) represents a probability distribution with PDF:*

$$\hat{f}_{\rho_{\mathbf{y}}}(\mathbf{y}) = \sum_{\ell=1}^m p_{\ell} \hat{f}_{\rho_{\mathbf{x}', \mathbf{y}'}}(\mathbf{y} | \mathbf{x}^{(\ell)}) \quad (12)$$

where

- $\hat{f}_{\rho_{\mathbf{x}', \mathbf{y}'}}(\mathbf{y} | \mathbf{x}^{(\ell)}) = \frac{\hat{f}_{\rho_{\mathbf{x}', \mathbf{y}'}}(\mathbf{x}^{(\ell)}, \mathbf{y})}{\int \hat{f}_{\rho_{\mathbf{x}', \mathbf{y}'}}(\mathbf{x}^{(\ell)}, \mathbf{y}) d\mathbf{y}}$  for  $k_{\mathbb{Y}} = k_{rbf}$
- $\hat{f}_{\rho_{\mathbf{x}', \mathbf{y}'}}(\mathbf{y} | \mathbf{x}^{(\ell)}) = \frac{\hat{f}_{\rho_{\mathbf{x}', \mathbf{y}'}}(\mathbf{x}^{(\ell)}, \mathbf{y})}{\sum_{i=1}^n \hat{f}_{\rho_{\mathbf{x}', \mathbf{y}'}}(\mathbf{x}^{(\ell)}, \mathbf{e}^{(i)})}$  for  $k_{\mathbb{Y}} = k_{cos}$

---

**Algorithm 1** Discriminative training

---

**input:** training dataset  $D = \{(\mathbf{x}^{(i)}, \mathbf{y}^{(i)})\}_{i=1 \dots \ell}$ , kernels  $k_{\mathbb{X}, \sigma}$  and  $k_{\mathbb{Y}}$  number of components  $m'$ , loss function  $\mathcal{L}$

- 1: Initialize  $C_{\mathbf{x}'\mathbf{y}'} \leftarrow \{(\mathbf{x}'^{(i)}, \mathbf{y}'^{(i)})\}_{i=1 \dots m'}$  with a random sample from  $D$
  - 2:  $\mathbf{p}_{\mathbf{x}'\mathbf{y}'} \leftarrow (\frac{1}{m'})_{i=1 \dots m'}$
  - 3:  $\rho_{\mathbf{x}'\mathbf{y}'} \leftarrow (C_{\mathbf{x}'\mathbf{y}'}, \mathbf{p}_{\mathbf{x}'\mathbf{y}'}, k_{\mathbb{X}, \sigma} \otimes k_{\mathbb{Y}})$
  - 4:  $\rho_{\mathbf{x}}^{(i)} \leftarrow (\{\mathbf{x}^{(i)}\}, (1), k_{\mathbb{X}, \sigma})$  for all  $i = 1 \dots \ell$  {create a kernel mixture for each input sample}
  - 5: **repeat**
  - 6:   Calculate  $\rho_{\mathbf{y}}^{(i)}$  using (11) with parameters  $\rho^{(i)}(\mathbf{x})$  and  $\rho(\mathbf{x}', \mathbf{y}')$  for all  $i = 1 \dots \ell$
  - 7:   Perform a step of gradient-based method to optimize:  $\min_{C_{\mathbf{x}'\mathbf{y}'}, \mathbf{p}_{\mathbf{x}'\mathbf{y}'}, \sigma} \sum_{i=1}^n \mathcal{L}(\rho_{\mathbf{y}}^{(i)}, \mathbf{y}^{(i)})$
  - 8: **until** stop criteria is met
  - 9: **return**  $\rho_{\mathbf{x}'\mathbf{y}'} = (C_{\mathbf{x}'\mathbf{y}'}, \mathbf{p}_{\mathbf{x}'\mathbf{y}'}, k_{\mathbb{X}} \otimes k_{\mathbb{Y}})$
- 

The parameters of the inference model correspond to the parameters of the QKM  $\rho_{\mathbf{x}'\mathbf{y}'}$ . This parameters can be estimated in three different ways:

- Non-parametric. Use the training dataset as the parameters of  $\rho_{\mathbf{x}'\mathbf{y}'}$  as described in Sect. 2.3. This leads to a memory-based learning method that may not scale well to large training datasets.
- Maximum likelihood learning. Estimate the parameters of  $\rho_{\mathbf{x}'\mathbf{y}'}$  by maximizing the probability density assigned by  $\rho_{\mathbf{x}'\mathbf{y}'}$  to the training dataset (Equation 6).
- Discriminative learning. Use (11) to perform a forward pass of an input kernel mixture  $\rho_x$  that can represent an individual sample (no uncertainty) or a distribution over the input space (uncertainty). Then, we minimize a suitable loss function (such as cross-entropy for classification or mean squared error for regression) with respect to the model parameters using gradient descent (Algorithm 2.5).

For discriminative learning, the loss function depends on the kind of output variable, which is determined by the kernel  $k_{\mathbb{Y}}$ . Given an output QKM  $\rho_{\mathbf{y}} = (\{\mathbf{y}'^{(i)}\}_{i=1 \dots m'}, (p_i'')_{i=1 \dots m'}, k_{\mathbb{Y}})$ , where  $k_{\mathbb{Y}} = k_{\text{cos}}$ , and a real output label  $\mathbf{y} \in \mathbb{R}^n$ , with  $\sum_{j=1}^n y_j = 1$  we can use, for instance, a cross-entropy loss:

$$\mathcal{L}_{\text{xe}}(\rho_{\mathbf{y}}, \mathbf{y}) = \text{CrossEntropy}(\boldsymbol{\pi}, \mathbf{y}), \quad (13)$$

where

$$\pi_j = \sum_{i=1}^{m'} p_i'' (\mathbf{y}_j^{(i)})^2, \text{ for } j = 1 \dots n \quad (14)$$

When  $k_{\mathbb{Y}} = k_{\text{rbf}}$ , we have a regression problem, in this case we can use a loss function such as mean square error:

$$\mathcal{L}_{\text{mse}}(\rho_{\mathbf{y}}, \mathbf{y}^{(i)}) = \text{mse}(\hat{\mathbf{y}}, \mathbf{y}^{(i)}), \quad (15)$$

where  $\hat{\mathbf{y}} = \sum_{j=1}^{m'} p_j'' \mathbf{y}_j^{(i)}$ .

## 2.6 Sampling from quantum kernel mixtures

Sampling from a QKM  $\rho_{\mathbf{x}} = (\{\mathbf{x}^{(i)}\}_{i=1 \dots m}, (p_i)_{i=1 \dots m}, k_{\text{rbf}, \sigma})$  with  $\mathbf{x}^{(i)} \in \mathbb{R}^n$  can be performed in two steps. First, draw a sample  $i'$  from a categorical distribution with probabilities  $(p_i)_{i=1 \dots m}$ . Second, draw a sample from a normal distribution  $\mathcal{N}(\mathbf{x}^{(i')}, 2\sigma \mathbf{I}_n)$ , where  $\mathbf{I}_n$  is the  $n$ -dimensional identity matrix.

To sample from a QKM  $\rho_{\mathbf{x}} = (\{\mathbf{x}^{(i)}\}_{i=1 \dots m}, (p_i)_{i=1 \dots m}, k_{\text{cos}})$ , we draw a sample from a categorical distribution with probabilities given by  $(\pi_j)_{j=1 \dots n}$ , where  $\pi_j$  is defined in the same way as in equation (14).

Sampling layers that sample from a QKM can also be included in a deep model. To maintain differentiability, we can use the Gumbel-softmax reparameterization for sampling categorical variables, as proposed by [19], along with the well-known reparameterization trick for Gaussian distributions. Another alternative is to use implicit reparameterization gradients, [20].

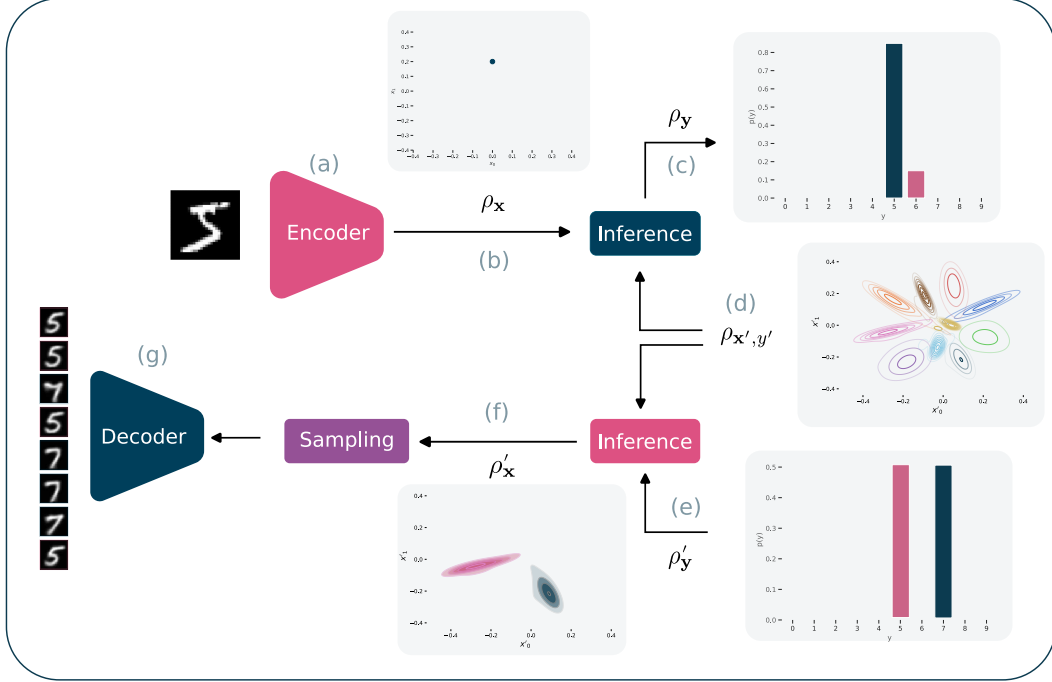


Figure 1: Classification and generation with QKMs. The top part represents a predictive model that uses an encoder (a) to map input samples into a latent space; the output of the encoder is represented as a QKM  $\rho_x$  (b) with one component, which is used to infer an output probability distribution of labels, represented by a QKM  $\rho_y$  (c), using (11); the classifier model has as a parameter a joint distribution of inputs and outputs, represented by a QKM  $\rho_{x',y'}$  (d), which is learned with algorithm 2.5. The joint probability can be used to do conditional generation, as depicted in the bottom of the diagram. In this case, the input is a distribution of labels represented by the QKM  $\rho'_y$  (e), which along with  $\rho_{x',y'}$  (d) is used to infer a predicted QKM  $\rho'_x$  using (11); we sample (f) from this QKM to generate input samples in the latent space which are decoded (g) to the original input space

### 3 Exploratory experiments

The purpose of this section is to demonstrate the framework’s capabilities through various learning tasks, rather than focusing solely on achieving competitive state-of-the-art performance. First, we present an example of a classification model based on the framework, highlighting the reversibility of kernel-mixture-based inference, which allows the model to function as both a classification and a conditional generative model. In the second example, we address the problem of learning from label proportions, where we lack individual training sample labels and have only the proportions of labels in sample bags. We treat this problem as an instance of input training sample uncertainty modeled with QKMs.

#### 3.1 Classification with quantum kernel mixtures

Figure 1 shows the task setup and models explored in this subsection. The upper part shows a classifier that combines a deep encoder,  $\Phi_\theta : \mathbb{X} \rightarrow \mathbb{R}^n$ , and a QKM inference module. The parameters of the model correspond to the joint QKM  $\rho_{x',y'} = (C_{x'y'}, p_{x'y'}, k_{\text{rbf},\sigma} \otimes k_{\text{cos}})$ , which represents the joint probability of the training input and output samples, and the parameters of the encoder,  $\theta$ . These parameters, together with the parameters of the encoder, are learned using an extended version of Algorithm 2.5 by minimizing the loss given by (13).

The lower part of Figure 1 shows a conditional-generative model that exploits the reversibility of the kernel mixture inference process (Eq. (11)). Thanks to the symmetry of 1, it is possible to use it to infer a probability distribution of inputs,  $\rho_x$ , given a probability distribution of outputs  $\rho_y$ . From this

Table 1: Classification accuracy comparison of the models on the three datasets: QKM classification model (QKM), QKM model fined-tuned for generation with maximum likelihood learning (ML-QKM), a baseline model with the same encoder coupled with a dense layer. Observe that the classification performance ML-QKM slightly degrades with respect to QKM, since a more faithful modeling of the input space distribution impacts the discriminative performance.

Dataset	QKM	ML-QKM	Encoder+Dense
Mnist	<b>0.993 ± 0.001</b>	<b>0.993 ± 0.001</b>	0.992 ± 0.001
Fashion-Mnist	<b>0.916 ± 0.004</b>	0.895 ± 0.004	0.907 ± 0.005
Cifar-10	<b>0.811 ± 0.005</b>	0.776 ± 0.012	0.810 ± 0.006

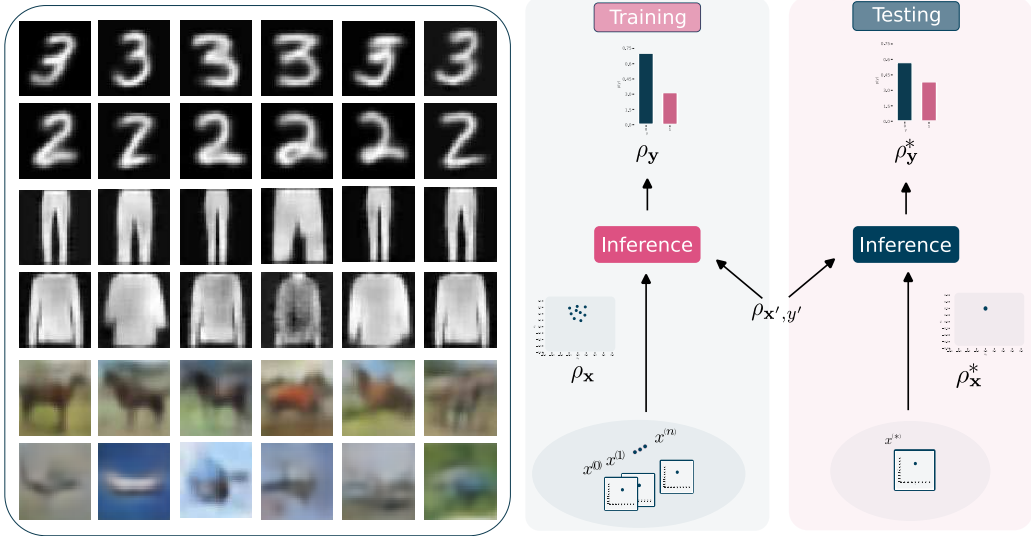


Figure 2: Left: image generation from Mnist, Fashion-Mnist, and Cifar-10 using QKM generative model, each row corresponds to an individual class. Right: illustration of the kernel-mixture-based model for classification with label proportions.

QKM we can draw samples (Subsect. 2.6) in the latent space, which can be mapped to the input space using a decoder  $\Psi_{\theta'} : \mathbb{R}^n \rightarrow \mathbb{X}$ . To improve the quality of the generated samples, the joint QKM  $\rho_{x', y'}$  is fine-tuned using maximum likelihood learning (see Subsect. 2.5) while keeping the parameters  $\theta$  of the encoder fixed. The parameters  $\theta'$  of the decoder are independently learned by training a conventional auto-encoder composed of  $\Phi_\theta$  and  $\Psi_{\theta'}$ , with the encoder parameters  $\theta$  fixed.

Table 1 shows the performance of the model on three benchmark datasets: MNIST, Fashion-MNIST and CIFAR-10. All models use a similar encoder architecture: a convolutional neural network (3 convolutional layers for MNIST and Fashion-MNIST, and 6 convolutional layers for CIFAR-10). As a baseline, we have coupled the encoder with a dense layer with approximately the same number of parameters as the QKM inference module (Encoder+Dense), so that we can compare QKM with a counterpart model of similar complexity. We also report the classification performance of the model before (QKM) and after performing the maximum likelihood fine tuning (ML-QKM) on the joint QKM  $\rho_{x', y'}$  for improving generation. Hyperparameter tuning of the models was performed using cross-validation on the training partition for each dataset. Ten experiments were run with the best hyperparameters, and the mean accuracy is reported along with the 99% confidence interval of a t-test. The results show that the performance of the QKM based model is on par with a deep model of comparable complexity.

The main advantage of the QKM -based model is the probabilistic modeling of the interaction between inputs and outputs, which is exploited by the conditional generative model. It uses the parameters learned by the ML-QKM to conditionally generate samples from the inferred probability distribution of the inputs. Some examples of conditionally generated samples for the three datasets are shown in the left part of Figure 2 .

Table 2: Performance evaluation for LLP tasks. Column headers indicate bag size. Values correspond to AUC plus a t-test 99% confidence interval.

Dataset, sampling	Method	8	32	128	512
Adult, $[0, \frac{1}{2}]$	LMMCM	0.8728 $\pm$ 0.0034	0.8693 $\pm$ 0.0084	0.8669 $\pm$ 0.0073	0.8674 $\pm$ 0.0072
	QKM	<b>0.8797 <math>\pm</math> 0.0054</b>	<b>0.8786 <math>\pm</math> 0.0048</b>	<b>0.8757 <math>\pm</math> 0.0056</b>	<b>0.8697 <math>\pm</math> 0.0038</b>
Adult, $[\frac{1}{2}, 1]$	LMMCM	0.8584 $\pm$ 0.0295	0.8644 $\pm$ 0.00937	0.8601 $\pm$ 0.00811	0.8500 $\pm$ 0.0335
	QKM	<b>0.8810 <math>\pm</math> 0.0083</b>	<b>0.8702 <math>\pm</math> 0.0121</b>	<b>0.8666 <math>\pm</math> 0.0081</b>	<b>0.8601 <math>\pm</math> 0.0073</b>
MAGIC, $[0, \frac{1}{2}]$	LMMCM	0.8909 $\pm$ 0.0013	<b>0.8799 <math>\pm</math> 0.0203</b>	<b>0.8753 <math>\pm</math> 0.0283</b>	<b>0.8734 <math>\pm</math> 0.0165</b>
	QKM	<b>0.8957 <math>\pm</math> 0.00132</b>	0.8766 $\pm$ 0.0083	0.8709 $\pm$ 0.0063	0.8578 $\pm$ 0.0043
MAGIC, $[\frac{1}{2}, 1]$	LMMCM	0.8911 $\pm$ 0.0149	0.8790 $\pm$ 0.0164	0.8684 $\pm$ 0.0083	0.8567 $\pm$ 0.0165
	QKM	<b>0.8957 <math>\pm</math> 0.0093</b>	<b>0.8793 <math>\pm</math> 0.0121</b>	<b>0.8709 <math>\pm</math> 0.0058</b>	<b>0.8578 <math>\pm</math> 0.045</b>

### 3.2 Classification with label proportions

Learning from label proportions (LLP) is a type of weakly supervised problem [21, 22]. In this scenario, instead of having explicit class labels for each training instance, we only have class proportions for subsets of training instances, called bags. The goal of the learner is to build a classifier that accurately labels individual instances. A bag of instances with label proportions can be thought of as a training sample that has uncertainty about the inputs and outputs, as discussed in Subsection 2.5. This uncertainty can be represented by QKMs as shown in the right-hand diagram in Figure 2. During training, the model receives as input bags of instances  $\mathbf{X}^{(i)} = (\mathbf{x}^{(i)j})_{j=1\dots m_i}$ . The training dataset corresponds to a set of pairs  $\mathbf{D} = (\mathbf{X}^{(i)}, \mathbf{y}^{(i)})_{i=1\dots \ell}$ , where each  $\mathbf{y}^{(i)}$  is a vector representing the label proportions of the  $i$ -th sample. Each input sample is represented by a QKM with  $m_i$  components. The algorithm 2.5 can be adapted to handle this bag representation by changing line 4 to  $\rho_{\mathbf{x}}^{(i)} \leftarrow (\mathbf{X}^{(i)}, (\frac{1}{m_i}, \dots, \frac{1}{m_i}), k_{\mathbb{X}})$ . The algorithm learns a joint QKM  $\rho_{\mathbf{x}', \mathbf{y}'}$ . During prediction, the model receives individual samples,  $x^{(*)}$ , which can be seen as bags with only one element. They are represented by a QKM  $\rho_{\mathbf{x}}^{(*)} = (\{x^{(*)}\}, \{1\}, k_{\mathbb{X}})$  with a unique component and uses 11, along with  $\rho_{\mathbf{x}', \mathbf{y}'}$ , to infer an output QKM  $\rho_y$ .

We compared this approach with a state-of-the-art LLP method based on a mutual contamination framework (LMMCM) [21]. We followed the same experimental setup as the one used by [21], where the authors built a set of bags of different sizes with the corresponding label proportions from a conventional classification dataset. The elements of the bags are sampled in such a way that the label proportions are iid uniform on  $[0, \frac{1}{2}]$  and on  $[\frac{1}{2}, 1]$ . The base datasets are Adult and MAGIC Gamma Ray Telescope from the UCI repository<sup>4</sup>.

Table 2 shows the evaluation of the LMMCM and the QKM methods using the area under the ROC curve (AUC) metric. The results are reported for different bag sizes, the two data sets, and the  $[0, \frac{1}{2}]$  and  $[\frac{1}{2}, 1]$  sampling schemes. The results show that QKM has a competitive performance equal to that of a state-of-the-art method explicitly designed for the LLP task. The good performance of QKM method is a result of its ability to naturally represent the uncertainty of the training samples.

## 4 Conclusions

The QKM framework presents a simple yet effective mechanism for representing joint probability distributions of both continuous and discrete random variables, providing a versatile tool for various machine learning tasks. The exploratory experiments shed light on the potential of this framework and show how it can be applied to diverse tasks such as conditional generation and weakly supervised learning. Quantum density matrices have long been used as the foundation of quantum mechanics, and their ability to blend linear algebra and probability is very attractive as a tool for machine learning. This work illustrates how such a formalism can be seamlessly and efficiently integrated with probabilistic deep learning models, opening up new avenues of research on the intersection of these fields.

<sup>4</sup><http://archive.ics.uci.edu/ml>

## 5 Limitations

While our research highlights the potential of QKM in machine learning, it also reveals certain limitations. First, density estimation methods may struggle with high-dimensional data; it is important to investigate how QKM is affected by increasing data dimensions. Second, the computational demands of integrating quantum density matrices with deep learning models may pose scalability challenges in large-scale applications. Finally, our study, being exploratory in nature, does not fully evaluate the applicability of QKM outside of conditional generation and weakly supervised learning, so this remains to be further explored.

## References

- [1] A. C. Damianou and N. D. Lawrence, “Deep Gaussian processes,” *Journal of Machine Learning Research*, vol. 31, pp. 207–215, 2013.
- [2] E. Goan and C. Fookes, “Bayesian Neural Networks: An Introduction and Survey,” *Lecture Notes in Mathematics*, vol. 2259, pp. 45–87, 2020.
- [3] I. Goodfellow, J. Pouget-Abadie, M. Mirza, B. Xu, D. Warde-Farley, S. Ozair, A. Courville, and Y. Bengio, “Generative adversarial networks,” *Communications of the ACM*, vol. 63, pp. 139–144, 10 2020.
- [4] D. P. Kingma and M. Welling, “Auto-Encoding Variational Bayes,” *2nd International Conference on Learning Representations, ICLR 2014 - Conference Track Proceedings*, 12 2013.
- [5] D. J. Rezende and S. Mohamed, “Variational inference with normalizing flows,” *32nd International Conference on Machine Learning, ICML 2015*, vol. 2, pp. 1530–1538, 2015.
- [6] G. Papamakarios, E. Nalisnick, D. J. Rezende, S. Mohamed, and B. Lakshminarayanan, “Normalizing Flows for Probabilistic Modeling and Inference,” *Journal of Machine Learning Research*, vol. 22, pp. 1–64, 2021.
- [7] P. Tiwari and M. Melucci, “Towards a Quantum-Inspired Binary Classifier,” *IEEE Access*, vol. 7, pp. 42354–42372, 2019.
- [8] G. Sergioli, E. Santucci, L. Didaci, J. A. Mischczak, and R. Giuntini, “A quantum-inspired version of the nearest mean classifier,” *Soft Computing*, vol. 22, pp. 691–705, 2 2018.
- [9] L. Wolf, “Learning using the Born Rule,” tech. rep., Massachusetts Institute of Technology Computer Science and Artificial Intelligence Laboratory, 2006.
- [10] Q. Li, D. Gkoumas, C. Lioma, and M. Melucci, “Quantum-inspired multimodal fusion for video sentiment analysis,” *Information Fusion*, vol. 65, pp. 58 – 71, 2021.
- [11] S. Srinivasan, C. Downey, and B. Boots, “Learning and Inference in Hilbert Space with Quantum Graphical Models,” *Advances in Neural Information Processing Systems*, vol. 2018-December, pp. 10338–10347, 10 2018.
- [12] F. A. González, A. Gallego, S. Toledo-Cortés, and V. Vargas-Calderón, “Learning with density matrices and random features,” *Quantum Machine Intelligence*, vol. 4, 12 2022.
- [13] A. Rahimi and B. Recht, “Random Features for Large-Scale Kernel Machines,” *Advances in Neural Information Processing Systems*, vol. 20, 2007.
- [14] M. A. Nielsen and I. L. Chuang, *Quantum Computation and Quantum Information*. Cambridge University Press, 6 2012.
- [15] M. Rosenblatt, “Remarks on some nonparametric estimates of a density function,” *The Annals of Mathematical Statistics*, vol. 27, no. 3, pp. 832–837, 1956.
- [16] E. Parzen, “On estimation of a probability density function and mode,” *The annals of mathematical statistics*, vol. 33, no. 3, pp. 1065–1072, 1962.
- [17] E. A. Nadaraya, “On Estimating Regression,” *Theory of Probability & Its Applications*, vol. 9, pp. 141–142, 1 1964.
- [18] G. S. Watson, “Smooth Regression Analysis,” *Sankhyā: The Indian Journal of Statistics, Series A (1961-2002)*, vol. 26, no. 4, pp. 359–372, 1964.

- [19] E. Jang, S. Gu, and B. Poole, “Categorical reparameterization with gumbel-softmax,” *5th International Conference on Learning Representations, ICLR 2017 - Conference Track Proceedings*, 2017.
- [20] M. Figurnov, S. Mohamed, and A. Mnih, “Implicit Reparameterization Gradients,” *Advances in Neural Information Processing Systems*, vol. 2018-December, pp. 441–452, 5 2018.
- [21] C. Scott and J. Zhang, “Learning from label proportions: A mutual contamination framework,” *Advances in Neural Information Processing Systems*, 2020.
- [22] J. Zhang, Y. Wang, and C. Scott, “Learning from Label Proportions by Learning with Label Noise,” *Advances in Neural Information Processing Systems*, vol. 35, pp. 26933–26942, 3 2022.

# Supplementary material

## 6 Proofs

**Proposition 2.2.** Let  $\rho_{\mathbf{x}} = (\mathbf{C}, \mathbf{p}, k_{\cos})$  be a QKM over  $\mathbb{R}^n$ ; let  $\mathbb{X} = \{\mathbf{b}^{(1)}, \dots, \mathbf{b}^{(n)}\} \subset \mathbb{R}^n$  be an orthogonal basis of  $\mathbb{R}^n$ , then  $\{f_{\rho}(\mathbf{b}^{(i)})\}_{i=1, \dots, n}$  is a categorical probability distribution for the random variable  $\mathbf{x} \in \mathbb{X}$ .

*Proof.* Let  $\mathbf{C} = \{\mathbf{x}^{(j)}\}_{j=1 \dots m}$ , then  $f_{\rho_{\mathbf{x}}}(\mathbf{b}^{(i)}) = \sum_{j=1}^m p_j \frac{\langle \mathbf{b}^{(i)}, \mathbf{x}^{(j)} \rangle^2}{\langle \mathbf{x}^{(j)}, \mathbf{x}^{(j)} \rangle} \geq 0$ .

$$\begin{aligned} \sum_{i=1}^n f_{\rho_{\mathbf{x}}}(\mathbf{b}^{(i)}) &= \sum_{i=1}^n \sum_{j=1}^m p_j \frac{\langle \mathbf{b}^{(i)}, \mathbf{x}^{(j)} \rangle^2}{\langle \mathbf{x}^{(j)}, \mathbf{x}^{(j)} \rangle} \\ &= \sum_{j=1}^m p_j \sum_{i=1}^n \frac{\langle \mathbf{b}^{(i)}, \mathbf{x}^{(j)} \rangle^2}{\langle \mathbf{x}^{(j)}, \mathbf{x}^{(j)} \rangle} \\ &= \sum_{j=1}^m p_j \left\| \frac{\mathbf{x}^{(j)}}{\langle \mathbf{x}^{(j)}, \mathbf{x}^{(j)} \rangle} \right\|^2 \quad (\mathbb{X} \text{ is a basis of } \mathbb{R}^n) \\ &= \sum_{j=1}^m p_j \\ &= 1 \end{aligned}$$

□

**Proposition 2.4.** Let  $\mathbb{X} = \{\mathbf{e}^{(1)}, \dots, \mathbf{e}^{(n)}\}$  be the canonical basis of  $\mathbb{R}^n$ ; let  $\mathbf{D} = \{\mathbf{x}^{(1)}, \dots, \mathbf{x}^{(\ell)}\} \subseteq \mathbb{R}^n$  be a set of iid samples drawn from  $\mathbb{X}$  with categorical probability distribution  $\mathbf{p} = (p_1, \dots, p_n)$ ; let  $\rho_{\mathbf{x}}^{\ell} = (\mathbf{D}, \mathbf{p} = (\frac{1}{\ell}, \dots, \frac{1}{\ell}), k_{\cos})$  be a QKM; and let  $\hat{f}_{\rho_{\mathbf{x}}^{\ell}}(\mathbf{x})$  be defined as in (5). Then  $\hat{f}_{\rho_{\mathbf{x}}^{\ell}}(\mathbf{e}^{(i)}) \rightarrow p_i$  as  $\ell \rightarrow \infty$ .

*Proof.*

$$\begin{aligned} f_{\rho_{\mathbf{x}}^{\ell}}(\mathbf{e}^{(i)}) &= \sum_{j=1}^{\ell} \frac{1}{\ell} k_{\cos}^2(\mathbf{x}^{(j)}, \mathbf{e}^{(i)}) \\ &= \sum_{j=1}^{\ell} \frac{1}{\ell} \langle \mathbf{x}^{(j)}, \mathbf{e}^{(i)} \rangle^2 \\ &= \sum_{j=1}^{\ell} \frac{1}{\ell} 1(\mathbf{x}^{(j)} = \mathbf{e}^{(i)}) \end{aligned}$$

Because of the large numbers law:

$$\lim_{\ell \rightarrow \infty} f_{\rho_{\mathbf{x}}^{\ell}}(\mathbf{e}^{(i)}) = \lim_{\ell \rightarrow \infty} \sum_{j=1}^{\ell} \frac{1}{\ell} 1(\mathbf{x}^{(j)} = \mathbf{e}^{(i)}) = E[1(\mathbf{x}^{(j)} = \mathbf{e}^{(i)})] = p_i \quad (16)$$

□

**Proposition 2.5.** Let  $\mathbf{x}'$  and  $\mathbf{y}'$  be random variables with joint a joint probability distribution represented by a QKM  $\rho_{\mathbf{x}', \mathbf{y}'}$  (Eq. (9)), and let  $\rho_{\mathbf{x}}$  be the QKM defined by (8), then the QKM  $\rho_{\mathbf{y}}$  (Eq. (10) and Eq. 11) represents a predicted probability distribution with PDF:

$$\hat{f}_{\rho_{\mathbf{y}}}(\mathbf{y}) = \sum_{\ell=1}^m p_{\ell} \hat{f}_{\rho_{\mathbf{x}', \mathbf{y}'}}(\mathbf{y} | \mathbf{x}^{(\ell)})$$

where

- $\hat{f}_{\rho_{\mathbf{x}'}, \mathbf{y}'}(\mathbf{y}|\mathbf{x}^{(\ell)}) = \frac{\hat{f}_{\rho_{\mathbf{x}'}, \mathbf{y}'}(\mathbf{x}^{(\ell)}, \mathbf{y})}{\int \hat{f}_{\rho_{\mathbf{x}'}, \mathbf{y}'}(\mathbf{x}^{(\ell)}, \mathbf{y}) d\mathbf{y}}$  for  $k_{\mathbb{Y}} = k_{\text{rbf}}$
- $\hat{f}_{\rho_{\mathbf{x}'}, \mathbf{y}'}(\mathbf{y}|\mathbf{x}^{(\ell)}) = \frac{\hat{f}_{\rho_{\mathbf{x}'}, \mathbf{y}'}(\mathbf{x}^{(\ell)}, \mathbf{y})}{\sum_{i=1}^n \hat{f}_{\rho_{\mathbf{x}'}, \mathbf{y}'}(\mathbf{x}^{(\ell)}, \mathbf{e}^{(i)})}$  for  $k_{\mathbb{Y}} = k_{\text{cos}}$

*Proof. Step 1.* Show that for both  $k_{\mathbb{Y}} = k_{\text{rbf}}$  and  $k_{\mathbb{Y}} = k_{\text{cos}}$

$$\hat{f}_{\rho_{\mathbf{x}'}, \mathbf{y}'}(\mathbf{y}|\mathbf{x}^{(\ell)}) = \frac{\hat{f}_{\rho_{\mathbf{x}'}, \mathbf{y}'}(\mathbf{x}^{(\ell)}, \mathbf{y})}{\mathcal{M}_{k_{\mathbb{X}}} \sum_{j=1}^{m'} p'_j k_{\mathbb{X}}^2(\mathbf{x}^{(\ell)}, \mathbf{x}'^{(j)})} \quad (17)$$

The case  $k_{\mathbb{Y}} = k_{\text{rbf}}$  follows from (7). For the case  $k_{\mathbb{Y}} = k_{\text{cos}}$  we have

$$\begin{aligned} \sum_{i=1}^n \hat{f}_{\rho_{\mathbf{x}'}, \mathbf{y}'}(\mathbf{x}^{(\ell)}, \mathbf{e}^{(i)}) &= \sum_{i=1}^n \sum_{j=1}^{m'} p'_j \mathcal{M}_{k_{\mathbb{X}}} \mathcal{M}_{k_{\text{cos}}} k_{\mathbb{X}}^2(\mathbf{x}^{(\ell)}, \mathbf{x}'^{(j)}) k_{\text{cos}}^2(\mathbf{e}^{(i)}, \mathbf{y}'^{(j)}) \\ &= \mathcal{M}_{k_{\mathbb{X}}} \sum_{j=1}^{m'} p'_j k_{\mathbb{X}}^2(\mathbf{x}^{(\ell)}, \mathbf{x}'^{(j)}) \sum_{i=1}^n k_{\text{cos}}^2(\mathbf{e}^{(i)}, \mathbf{y}'^{(j)}) \\ &= \mathcal{M}_{k_{\mathbb{X}}} \sum_{j=1}^{m'} p'_j k_{\mathbb{X}}^2(\mathbf{x}^{(\ell)}, \mathbf{x}'^{(j)}) \end{aligned}$$

**Step 2,** Use the derivation above to prove the main result:

$$\begin{aligned} \hat{f}_{\rho_{\mathbf{y}}}(\mathbf{y}) &= \mathcal{M}_{k_{\mathbb{Y}}} \sum_{i=1}^{m'} p''_i k_{\mathbb{Y}}^2(\mathbf{y}, \mathbf{y}'^{(i)}) && \text{(use Eq. (4))} \\ &= \mathcal{M}_{k_{\mathbb{Y}}} \sum_{i=1}^{m'} \sum_{\ell=1}^m \frac{p_{\ell} p'_i k_{\mathbb{X}}^2(\mathbf{x}^{(\ell)}, \mathbf{x}'^{(i)})}{\sum_{j=1}^{m'} p'_j k_{\mathbb{X}}^2(\mathbf{x}^{(\ell)}, \mathbf{x}'^{(j)})} k_{\mathbb{Y}}^2(\mathbf{y}, \mathbf{y}'^{(i)}) && \text{(use Eq. (11))} \\ &= \sum_{\ell=1}^m p_{\ell} \frac{\mathcal{M}_{k_{\mathbb{X}}} \mathcal{M}_{k_{\mathbb{Y}}} \sum_{i=1}^{m'} p'_i k_{\mathbb{X}}^2(\mathbf{x}^{(\ell)}, \mathbf{x}'^{(i)}) k_{\mathbb{Y}}^2(\mathbf{y}, \mathbf{y}'^{(i)})}{\mathcal{M}_{k_{\mathbb{X}}} \sum_{j=1}^{m'} p'_j k_{\mathbb{X}}^2(\mathbf{x}^{(\ell)}, \mathbf{x}'^{(j)})} \\ &= \sum_{\ell=1}^m p_{\ell} \frac{\hat{f}_{\rho_{\mathbf{x}'}, \mathbf{y}'}(\mathbf{x}^{(\ell)}, \mathbf{y})}{\mathcal{M}_{k_{\mathbb{X}}} \sum_{j=1}^{m'} p'_j k_{\mathbb{X}}^2(\mathbf{x}^{(\ell)}, \mathbf{x}'^{(j)})} \\ &= \sum_{\ell=1}^m p_{\ell} \hat{f}_{\rho_{\mathbf{x}'}, \mathbf{y}'}(\mathbf{y}|\mathbf{x}^{(\ell)}) && \text{(use Eq. (17))} \end{aligned}$$

□

## 7 Algorithms

This section includes algorithms that make explicit some calculations that are implicit in the main text.

---

### Algorithm 2 Inference with kernel mixtures

---

**input:** Input kernel mixture  $\rho_{\mathbf{x}} = (\{\mathbf{x}^{(i)}\}_{i=1\dots m}, (p_i)_{i=1\dots m}, k_{\mathbb{X}})$ , joint kernel mixture  $\rho_{\mathbf{x}', \mathbf{y}'} = (\{\mathbf{x}'^{(i)}, \mathbf{y}'^{(i)}\}_{i=1\dots m'}, (p'_i)_{i=1\dots m'}, k_{\mathbb{X}} \otimes k_{\mathbb{Y}})$

- 1:  $\mathbf{C}_{\mathbf{y}} \leftarrow \{\mathbf{y}'^{(i)}\}_{i=1\dots m'}$
  - 2:  $\mathbf{p}_{\mathbf{y}} \leftarrow (p''_k)_{k=1\dots m'}$  where  $p''_k$  is calculated using (11)
  - 3: **return**  $\rho_{\mathbf{y}} = (\mathbf{C}_{\mathbf{y}}, \mathbf{p}_{\mathbf{y}}, k_{\mathbb{Y}})$
-

---

**Algorithm 3** Maximum likelihood training

---

**input:** training dataset  $D = \{(\mathbf{x}^{(i)}, \mathbf{y}^{(i)})\}_{i=1\dots\ell}$ , kernels  $k_{\mathbb{X}}$  and  $k_{\mathbb{Y}}$ , number of components  $m'$

- 1: Initialize  $C_{\mathbf{x}'\mathbf{y}'} = \{(\mathbf{x}'^{(i)}, \mathbf{y}'^{(i)})\}_{i=1\dots m'}$  with a random sample from  $D$
- 2: Initialize  $\mathbf{p}_{\mathbf{x}'\mathbf{y}'} \leftarrow (\frac{1}{m'})_{i=1\dots m'}$
- 3:  $\rho_{\mathbf{x}',\mathbf{y}'} = (C_{\mathbf{x}'\mathbf{y}'}, \mathbf{p}_{\mathbf{x}'\mathbf{y}'}, k_{\mathbb{X}} \otimes k_{\mathbb{Y}})$
- 4: Use gradient-based optimization to find:

$$\max_{C_{\mathbf{x}'\mathbf{y}'}, \mathbf{p}_{\mathbf{x}'\mathbf{y}'}, \theta} \sum_{i=1}^{\ell} \log \hat{f}_{\rho_{\mathbf{x}'\mathbf{y}'}}(\mathbf{x}^{(i)}, \mathbf{y}^{(i)})$$

- 5: **return**  $\rho_{\mathbf{x}',\mathbf{y}'} = (C_{\mathbf{x}'\mathbf{y}'}, \mathbf{p}_{\mathbf{x}'\mathbf{y}'}, k_{\mathbb{X}} \otimes k_{\mathbb{Y}})$
- 

---

**Algorithm 4** Discriminative training with bags of instances

---

**input:** training dataset  $D = \{(\mathbf{X}^{(i)}, \mathbf{y}^{(i)})\}_{i=1\dots\ell}$  with  $\mathbf{X}^{(i)} = (\mathbf{x}^{(i)j})_{j=1\dots m_i}$ , kernels  $k_{\mathbb{X},\sigma}$  and  $k_{\mathbb{Y}}$ , number of components  $m'$ , loss function  $\mathcal{L}$

- 1: Initialize  $C_{\mathbf{x}'\mathbf{y}'} \leftarrow \{(\mathbf{x}'^{(i)}, \mathbf{y}'^{(i)})\}_{i=1\dots m'}$  with a random sample from  $D$
  - 2:  $\mathbf{p}_{\mathbf{x}'\mathbf{y}'} \leftarrow (\frac{1}{m'})_{i=1\dots m'}$
  - 3:  $\rho_{\mathbf{x}',\mathbf{y}'} \leftarrow (C_{\mathbf{x}'\mathbf{y}'}, \mathbf{p}_{\mathbf{x}'\mathbf{y}'}, k_{\mathbb{X},\sigma} \otimes k_{\mathbb{Y}})$
  - 4:  $\rho_{\mathbf{x}}^{(i)} \leftarrow (\mathbf{X}^{(i)}, (\frac{1}{m_i}, \dots, \frac{1}{m_i}), k_{\mathbb{X}})$  for all  $i = 1 \dots \ell$
  - 5: **repeat**
  - 6: Calculate  $\rho_{\mathbf{y}}^{(i)}$  using (11) with parameters  $\rho^{(i)}(\mathbf{x})$  and  $\rho(\mathbf{x}', \mathbf{y}')$  for all  $i = 1 \dots \ell$
  - 7: Perform a step of gradient-based method to optimize:  $\min_{C_{\mathbf{x}'\mathbf{y}'}, \mathbf{p}_{\mathbf{x}'\mathbf{y}'}, \sigma} \sum_{i=1}^n \mathcal{L}(\rho_{\mathbf{y}}^{(i)}, \mathbf{y}^{(i)})$
  - 8: **until** stop criteria is met
  - 9: **return**  $\rho_{\mathbf{x}',\mathbf{y}'} = (C_{\mathbf{x}'\mathbf{y}'}, \mathbf{p}_{\mathbf{x}'\mathbf{y}'}, k_{\mathbb{X}} \otimes k_{\mathbb{Y}})$
- 

## 8 Experimental Setup

In this subsection, we provide a comprehensive description of our experimental setup to ensure reproducibility.

### 8.1 Hardware Specifications

Our experiments were conducted using a server that incorporates a 64-core Intel Xeon Silver 4216 CPU 2.10 GHz processor, 128 GB of RAM, and two NVIDIA RTX A5000 GPUs.

### 8.2 Classification with quantum kernel mixtures

Three different models were assessed in this experiment as explained in Subsection 3.1: QKM classification model (QKM), QKM model fined-tuned for a generation with maximum likelihood learning (ML-QKM), and a baseline model with the same encoder coupled with a dense layer. The encoder model utilized for both MNIST and Fashion-MNIST datasets was identical. It consisted of the following components:

- Lambda Layer: The initial layer converted each sample into a 32-float number and subtracted 0.5 from it.
- Convolutional Layers: Two convolutional layers were appended, each with 32 filters, 5-kernel size, same padding, and strides 1 and 2, respectively. Subsequently, two more convolutional layers were added, each with 64 filters, 5-kernel size, same padding, and strides 1 and 2, respectively. Finally, a convolutional layer with 128 filters, 7-kernel size, and stride 1 was included. All convolutional layers employed the Gaussian Error Linear Unit (GELU) activation function.
- Flattened Layer: The output from the previous layer was flattened.

- Dropout Layer: A dropout layer with a dropout rate of 0.2 was introduced.
- Dense Layer: The subsequent dense layer's neuron encoding size was determined using a grid hyperparameter search in the range of  $2^i$ , where  $i \in \{1, \dots, 7\}$ .

The decoder architecture consisted of the following components:

- Reshape Layer: The input to the decoder passed through a reshape layer.
- Convolutional Layers: Three convolutional layers were employed, each with 64 filters and kernel sizes of seven, five, and five, respectively. The strides for these layers were set to 1, 1, and 2, while the padding was configured as valid, same, and same, respectively.
- Additional Convolutional Layers: Subsequently, three more convolutional layers were utilized, each with 32 filters, 5-kernel size, and strides 1, 2, and 1, respectively. All these layers utilized the Gelu activation function and had padding set to "same."
- Final Convolutional Layer: The decoder concluded with a 1-filter convolutional layer employing same padding.

Similar to the encoder, all layers in the decoder employed the GELU activation function.

For Cifar-10 a different encoder was used for

- Convolutional Layers: The input tensor is passed through a series of convolutional layers. Each layer applies a 3x3 kernel to extract features from the input. The activation function used is the GELU. Padding is set to 'same'. Batch normalization is applied after each convolutional layer to normalize the activations.
- Max Pooling: After each pair of convolutional layers, max pooling is performed using a 2x2 pool size.
- Encoding Layer: The feature maps obtained from the previous layers are flattened into a vector representation using the Flatten layer.
- Dropout: A dropout layer with a dropout rate of 0.2 is added.
- Hidden Layer: A dense layer of variable size is introduced to further transform the encoded features. The size is search
- Dropout: Another dropout layer with a dropout rate of 0.2 is added after the hidden layer

The decoder architecture for Cifar-10 consisted of the following components:

- Dense Layer: The input tensor is passed through a dense layer that restores the tensor to its original size.
- Reshape Layer: The tensor is reshaped to match the spatial dimensions of the original input using the Reshape layer.
- Convolutional Transpose Layers: The reshaped tensor undergoes a series of convolutional transpose layers. Each layer applies a 3x3 kernel to upsample the feature maps. The activation function used is 'gelu'. Padding is set to 'same' to maintain the spatial dimensions.
- Batch Normalization: Batch normalization is applied after each convolutional transpose layer to normalize the activations.
- Upsampling: UpSampling2D layers with a size of (2, 2) are used to increase the spatial dimensions of the feature maps.
- Final Convolutional Transpose Layer: The last convolutional transpose layer reconstructs the original number of channels in the input data. Padding is set to 'same'.
- Activation Function: The final output is passed through an activation function, sigmoid; to ensure the reconstructed data is within the appropriate range.

The number of components in every dataset for the QKM classification model was searched in  $2^i$ , where  $i \in \{2, \dots, 10\}$ . The same for ML-QKM. For the baseline model, the dense layer was searched using the same number of parameters that the QKM classification model generates. The best parameters can be found in Table 8.2.

The results reported in Table 1 were generated by running each algorithm in each dataset ten times and averaging their results.

Table 3: Best parameters for the classification with quantum kernel mixture experiment.

Dataset	QKM		QKM-ML		Baseline Dense Layer	
	Number of Components	Encoded Size	Number of Components	Encoded Size	Number of Components	Encoded Size
Mnist	512	128	512	128	8	8
Fashin-Mnist	256	128	256	128	4	16
Cifar-10	1024	32	1024	32	4	64

### 8.3 Classification with label proportions

The experimental setup of this experiment is based on the work of Scott et al. [21]. The study utilizes two datasets, namely Adult (T = 8192) and MAGIC Gamma Ray Telescope (T = 6144), both obtained from the UCI repository.<sup>5</sup> For each dataset, the authors created datasets with bags of instances with different proportions of LPs. Each dataset has its distribution of label proportions (LPs), and a bag size parameter, denoted as 'n'. The total number of training instances denoted as 'T', is fixed for each dataset, resulting in T/n bags. The LPs for the experiments are independently and uniformly distributed within the ranges  $[0, 1/2]$  and  $[1/2, 1]$ . The bag sizes considered are  $n = \{8, 32, 128, \text{ and } 512\}$ . Consequently, there are a total of 16 experimental configurations (2 LP distributions x 2 datasets x 4 bag sizes). For each configuration, 5 different pairs of training and test sets were created. Results are reported as the average of the AUC over the five test sets of each configuration. The numerical features in both datasets are standardized to have a mean of 0 and a variance of 1, while the categorical features are encoded using one-hot encoding. Hyperparameters are found using a validation subset (10%) of each training set. The best hyperparameters for each configuration are reported in Table 4

Table 4: Best hyper-parameters for the learning with label proportion experiment using QKM Model.

Dataset, sample	Bag Size	Num. Components	Learning Rate
Adult, $[0, \frac{1}{2}]$	8	32	0.005
Adult, $[0, \frac{1}{2}]$	32	16	0.001
Adult, $[0, \frac{1}{2}]$	128	512	0.001
Adult, $[0, \frac{1}{2}]$	512	64	0.005
Adult, $[\frac{1}{2}, 1]$	8	16	0.005
Adult, $[\frac{1}{2}, 1]$	32	64	0.001
Adult, $[\frac{1}{2}, 1]$	128	128	0.001
Adult, $[\frac{1}{2}, 1]$	512	64	0.005
MAGIC, $[0, \frac{1}{2}]$	8	256	0.005
MAGIC, $[0, \frac{1}{2}]$	32	128	0.005
MAGIC, $[0, \frac{1}{2}]$	128	128	0.001
MAGIC, $[0, \frac{1}{2}]$	512	256	0.001
MAGIC, $[\frac{1}{2}, 1]$	8	16	0.005
MAGIC, $[\frac{1}{2}, 1]$	32	128	0.005
MAGIC, $[\frac{1}{2}, 1]$	128	32	0.005
MAGIC, $[\frac{1}{2}, 1]$	512	128	0.001

### 8.4 Code

The code repository includes a comprehensive README.md file, providing detailed instructions to reproduce the results presented in this manuscript. To facilitate easy access, the pretraining weights of the best models for each experiment have been compressed into a zip file, which is publicly available for download from a designated location on Google Drive.

For conducting experiments involving learning with label proportions, as mentioned above, we have relied on the work of Scott et al. [21]. The authors made

<sup>5</sup><http://archive.ics.uci.edu/ml>.

the code available at this GitHub repository <https://github.com/Z-Jianxin/Learning-from-Label-Proportions-A-Mutual-Contamination-Framework>. Additionally, we have shared a compressed folder on Google Drive that contains the preprocessed data obtained using the scripts provided in the aforementioned project.